JOURNAL OF SPACECRAFT AND ROCKETS
Vol. 31, No. 1, January–February 1994

Particle Simulation of Rarefied Aeropass Maneuvers of the Magellan Spacecraft

Brian L. Haas*
Eloret Institute, Palo Alto, California 94303
and
William J. Feiereisen†
NASA Ames Research Center, Moffett Field, California 94035

Rarefied and free molecular flowfields corresponding to proposed aeropass maneuvers through the atmosphere of Venus by the Magellan spacecraft are computed with a vectorized particle simulation method. The significance of flow rarefaction, surface recombination, grid resolution, and simulation domain is assessed, and surface heat flux, drag, and flowfield properties are computed. A simple surface heat transfer model is coupled directly to the simulation and assumes that each surface element is in radiative equilibrium with deep space. This allows direct computation of surface temperature distributions rather than requiring prescribed isothermal estimates employed in previous particle methods. Uncoupled dual-node heat transfer models, which account for heat capacity and thermal conductivity within each structural component, permit more accurate determination of surface temperatures. Such temperatures restrict the allowable altitudes and entry speeds of the aeropass maneuvers and may influence vehicle aerodynamics and heating in rarefied flows. Simulations with an entry velocity of 8600 m/s at altitudes between 125 and 140 km reveal that allowable surface temperatures occur only at the highest altitudes where the flowfield is nearly free molecular. Excessive surface heat flux occurs at lower altitudes where molecular collisions are significant. Simulations employing insufficient upstream domain length overpredicted heating and drag.

Nomenclature

C_D = drag coefficient
c = heat capacity of material, J/m^2-K
D_{HGA} = diameter of high-gain antenna
E = molecular thermal or bond energy
Kn = Knudsen number
k = Boltzmann constant, 1.3805×10^{-23} J/K
M = Mach number
m = molar mass, g/mole
$\dot{N}$ = particle flux per unit surface area, m^{-2}-s^{-1}
n = number density, m^{-3}
Q_∞ = freestream energy flux, $\rho_\infty u_\infty^3/2$
$\dot{q}$ = heat flux per unit surface area, W/m^2
S = number of species in gas mixture
T = temperature, K
t = time, s
u = flow velocity, m/s
α = intermolecular potential exponent
ϵ = surface radiative emissivity
ζ = number of thermal degrees of freedom
θ_v = characteristic vibrational temperature, K
κ = thermal conductivity of material, W/m^2-K
λ = gas mean free path, m
ρ = gas density, kg/m^3
σ = Stefan-Boltzmann constant, 5.67×10^{-8} W/m^2-K^4
τ = duration of heating pulse, s

Subscripts

a, b = front and back nodes of plate, respectively
inc = incident flux
int = internal energy
j = species j
r = rotational mode
refl = reflected flux
rxn = chemical reactions
s = surface quantity
t = simulation time step
v = vibrational mode
0 = initial or deep-space value
∞ = freestream value

Received April 20, 1992; revision received Jan. 8, 1993; accepted for publication Feb. 17, 1993.

*Research Scientist; mailing address: NASA Ames Research Center, M/S 230-2, Moffett Field, CA 94035-1000. Member AIAA.
†Research Scientist. Member AIAA.

Introduction

THE highly elliptic orbit of the Magellan spacecraft about Venus was circularized through a series of aerobrake maneuvers in the summer of 1993. The Magellan spacecraft, employing a synthetic array radar, had been mapping the surface of Venus since September 15, 1990. Mission engineers at the Jet Propulsion Laboratory (JPL) favored a circular orbit to improve the resolution of radar images and the measured gravity field.[1] However, to circularize the current polar orbit of large eccentricity (0.39) required a significant reduction in vehicle velocity ($\Delta u = -1260$ m/s) from the original velocity of roughly 8600 m/s at periapsis. There was insufficient fuel on board the spacecraft to accomplish the orbital maneuver using propulsion systems alone. Alternatively, a series of aerobrake maneuvers through the atmosphere of Venus provided sufficient drag to reduce vehicle velocity. Limited propulsive fuel was needed only to initiate, control, and terminate the series of aerobraking maneuvers. Since the spacecraft was not designed for aerobraking, each pass through the atmosphere was restricted to prevent excessive heating of delicate body surfaces. However, mission objectives constrained the duration of the complete aerobraking process to about 70 days. Balancing these constraints suggests employing roughly 840 successive aeropasses with each pass yielding a reduction in velocity of about 1.5 m/s. A more complete discussion of the maneuver is presented in Ref. 1.

For vehicles encountering free molecular flow, heating of body surfaces may be estimated accurately with the ray-tracing and analytic techniques employed in the FREEMAC code.[2] Such flow conditions apply at high altitudes where the mean free path is large

in comparison with body dimensions (large Knudsen number *Kn*). However, at lower altitudes, characterized by greatly increased freestream densities, a concentration of molecules just ahead of body surfaces will lead to molecular collisions with freestream molecules. These collisions permit an exchange of freestream energy to the gas concentrated near the body, thus reducing the net energy flux into body surfaces. Flowfield computation methods based on the free molecular flow assumption are no longer appropriate to capture surface heating under these rarefied conditions. However, at altitudes of interest to the proposed Magellan maneuver, the flowfield is sufficiently rarefied ($Kn > 0.1$) that continuum methods are inapplicable as well. Alternatively, direct particle simulation methods are particularly well suited for computing rarefied flows by modeling the flow as a collection of moving and colliding discrete particles in accordance with kinetic theory and statistical mechanics.

The objective of the present study was to simulate rarefied flows about the Magellan spacecraft during aeropass maneuvers with a particle simulation method developed by Baganoff and McDonald[3] and McDonald.[4] The primary goals were to assess the significance of rarefaction effects on the net energy flux encountered by body surfaces and to provide corresponding estimates of surface heating, temperatures, and drag characteristics. Solutions were generated for entry at zero pitch and yaw over a range of altitudes from 125 to 140 km. Similar studies by Raulf[5] investigated aerodynamic loads over many pitch and roll angles at 140 km only. In this paper, the fundamentals of the particle simulation method are introduced, followed by discussion of the specifications employed in simulating the Magellan flow, including body geometry, flowfield conditions, and models for surface heat transfer and molecular interactions. Results are then presented for each periapsis altitude.

Particle Simulation Fundamentals

Particle simulation methods fundamentally decouple molecular motion from molecular interaction.[6] Given a particular position, velocity, and internal energy status, each particle in the flowfield travels unobstructed along the linear trajectory of its velocity vector over the duration of a single time step. At this time, neighboring particles are identified throughout the flowfield and paired off as potential collision candidates. The flowfield is divided into a network of cells to facilitate identification of neighboring particles and to define the finest resolution for sampling macroscopic flow properties. Employing probabilities as functions of individual collision parameters such as collision cross section and relative translational speed,[3] the subset of all candidate pairs that collide during the time step is identified. Nonreactive colliding particles may experience thermal collision mechanics that may include rotational and vibrational relaxation.[7,8] In simulating free molecular flow, the probability of collision is artificially set to zero, representing an infinite molecular mean free path.

The entire simulated flowfield is initialized with freestream conditions. The particle simulation then runs through a transient phase as the solution develops and flowfield structures form. Upon reaching steady state, the simulation collects statistical samples for measuring properties of the flowfield and body surfaces.

The code employed in the present study was developed by McDonald[4] for efficient implementation on Cray supercomputers. This code simulates nonreactive, three-dimensional flow of general gas mixtures about arbitrary geometries.

Particle Interaction Model

A simulated particle may contain energy in both translational and internal energy modes. The molecular collision rate and corresponding mean free path in the flowfield are dependent on relative translational energies among the particles and the assumed intermolecular potential. The variable hard sphere model[3,9] employed here assumes that the collision rate of neighboring particles corresponds to the inverse power-law intermolecular potential of exponent α. Appropriate values of α lie between the Maxwell molecule limit ($\alpha = 4$) and the hard sphere limit ($\alpha = \infty$) and are determined typically from viscosity behavior of the gas. Isotropic scattering, akin to the mechanics of hard sphere interactions, is employed to model the outcome of particle collisions.

Internal Energy Model

Internal energy modes absorb some flowfield energy that might otherwise be transferred to a body surface. In the present study, a fixed fraction ($^1/_5$) of colliding particles also experiences exchanges of energy between the internal energy modes and the relative translational energy. The combined influence of rotational, vibrational, and electron energy modes may be modeled in the simulation by assigning a fixed number of degrees of freedom for internal energy ζ_{int}. At equilibrium temperature T, the average energy E contained in any given energy mode of a molecule is proportional to the corresponding number of degrees of freedom,

$$E = \frac{\zeta}{2} kT \tag{1}$$

Translational energy has three degrees of freedom corresponding to motion along each of the principle axes. Linear polyatomic molecules have two degrees of freedom in rotation ($\zeta_r = 2$) when fully excited.

The vibrational modes of polyatomic molecules are typically partially excited due to large characteristic vibrational temperatures θ_v in comparison to flowfield temperatures. For simple harmonic oscillators of quantum energy $k\theta_v$, the effective continuous number of degrees of freedom ζ_v describing the vibrational mode is given by

$$\zeta_v = 2\frac{\theta_v/T}{\exp(\theta_v/T) - 1} \tag{2}$$

Simple diatomic molecules such as N_2 and CO have only one vibrational mode and therefore only one characteristic quantum energy. However, CO_2 has four vibrational and bending modes leading to four characteristic quantum energies. Rather than account for each of these energies independently in the simulation, it suffices to lump the rotational and vibrational energies into a single, continuous, internal energy with a corresponding number of degrees of freedom, given for the gas mixture as follows:

$$\zeta_{\text{int}} = \sum_{j=1}^{s} \frac{n_j}{n} (\zeta_r + \zeta_{v1} + \zeta_{v2} + \cdots)_j \tag{3}$$

When the expression in Eq. (3) is used, it is appropriate to approximate the contribution of the internal energy modes of the gas mixture with a fixed number of internal degrees of freedom, $\zeta_{\text{int}} = 3$. Energy exchanges among the internal modes are accomplished with the standard method of Borgnakke and Larsen.[10]

Spacecraft Surface Models

The geometry of the Magellan spacecraft is shown in Fig. 1 and compared with the simulated geometry employed at 125 km. The proposed aeropass maneuver would orient the vehicle at periapsis with the concave blanket of the solid rocket motor shell (SRM) forward and the high-gain antenna (HGA) aft. Because of the large mean free path in the flow about the spacecraft, small features on the vehicle, such as the altimeter antenna (ALTA), the medium-gain (MGA) and low-gain antennas (LGA), and the rocket engine modules (REM), have negligible impact on the flowfield as a whole and may be excluded to simplify the simulation geometry. Most importantly, this leads to a vehicle with two planes of symmetry, requiring simulation of only one-quarter of the entire vehicle geometry, thus reducing the computational expense of the simulation. In addition to the SRM and HGA, the simulated geometry in Fig. 1 includes solar panels (PAN), a cylindrical equipment bus (BUS), and the forward equipment module (FEM).

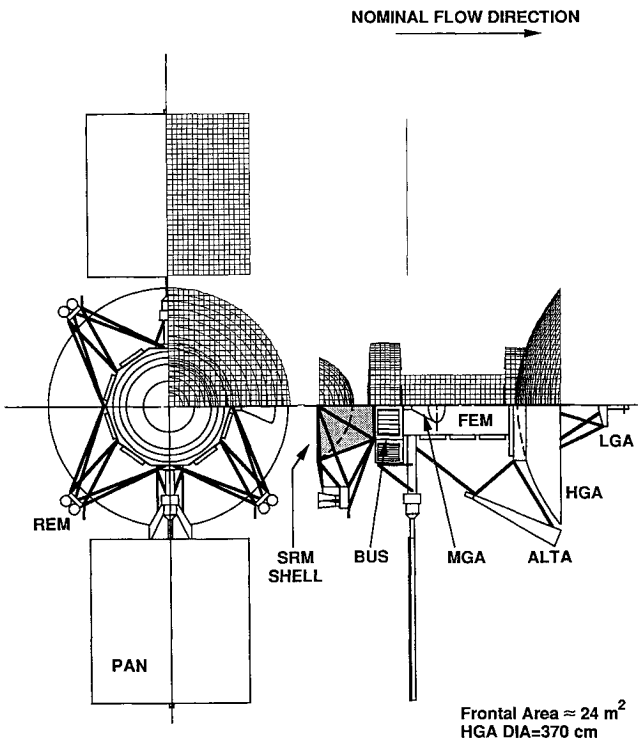

Fig. 1 Magellan spacecraft configuration vs simulated geometry employing one quadrant of the vehicle. Grid resolution corresponds to simulation at 125 km.

To represent a surface in the cubic Cartesian grid network of the simulation, it is necessary to approximate the surface as a composite of planar facets. Each facet has a normal defined from the intersections of the surface with the edges of the cell. This faceted description of the body is appropriate given that body radii are large in comparison with the cell size and that the intersection of different surfaces occurs at cell boundaries.

In particle methods, grid resolution must insure that cells are less than roughly one local mean free path length in size to compute surface heating and drag accurately.[11] Gas density builds near the body surface for cold-wall blunt-body flows, leading to very short local mean free paths compared with the freestream. An appropriate estimate for λ is given by Bird[12] as follows:

$$\frac{\lambda}{\lambda_\infty} = \frac{n_\infty}{n}\left(\frac{T}{T_\infty}\right)^{2/\alpha} \tag{4}$$

For each altitude, the corresponding grid resolution employed in the present work insured that the cell dimension was within roughly one stagnation mean free path at the solar panels. Since these panels are a dominant component of the structure, the simulation cell network was scaled such that the square simulated panels and the HGA had the same frontal areas as the actual vehicle components. Note that body dimensions that fail to lie on cell boundaries do not match the specified configuration exactly. This is insignificant since most of these dimensions do not affect the frontal area of the vehicle.

The simulated flowfield configuration is that of a wind tunnel with specularly reflecting symmetry planes and free molecular top and side planes. Particles that collide with the free molecular planes will reflect specularly unless they have already hit the spacecraft body, in which case they are removed from the simulation. This closely simulates highly rarefied or free molecular flow conditions by removing the influence of the tunnel walls on the flowfield. For highly rarefied flows, failure to employ an upstream domain of sufficient length leads to overprediction of vehicle heating and drag. Quoted in units of HGA diameters, D_{HGA}, the upstream boundries in the present studies were at a distance of at least $6D_{HGA}$ ahead of the solar panels. The top, side, and downstream boundaries of the simulated tunnel were each a distance of $D_{HGA}/3$ away from the body.

Radiative-Equilibrium Surface Heat Transfer Model

Surface temperatures can have a dramatic influence on vehicle aerodynamics in rarefied flows. Body surfaces are modeled in the present work as if in radiative equilibrium with deep space at a temperature of $T_0 = 4$ K. That is, the net influx of energy convected by flowfield particles through that surface facet of area A equals the energy that would radiate with emissivity ϵ from that surface facet at temperature T_s. Given that surface temperatures remain low (below 1000 K) and that none of the surfaces are particularly smooth, it is assumed that the surface accommodation coefficient is unity.[13] The surface facets corresponding to thin components (PAN, HGA, SRM) radiate on both sides, doubling the effective radiative surface area. All other surfaces radiate in the normal direction only. This model is simple to implement in the simulation, it does not require a prescribed estimate of surface temperature, and it allows each surface facet to reach its own temperature independent of neighboring facets. It is assumed that radiation from cool body surfaces would contribute negligibly to the net heating of the delicate hot surfaces of interest. Likewise, heating of the flow directly from surface radiation would be minimal and is neglected.

The equation describing conservation of energy for a surface facet in radiative equilibrium at surface temperature T_s with deep space at temperature T_0, given that the surface absorbs the incident particle energy flux per area $\dot{q}_{inc}$ and reflects all particles fully accommodated to the surface, is written as follows:

$$q_{inc} - \dot{N}_{inc}\frac{\zeta}{2}kT_s - \epsilon\sigma(T_s^4 - T_0^4) = 0 \tag{5}$$

where ζ is the number of degrees of freedom pertaining to reflected particles ($\zeta = 4 + \zeta_{int}$).

In the simulation, the particle energy influx $\dot{q}_{inc}$ could be measured directly for each facet. Rather than solving the fourth-order polynomial for surface temperature T_s from Eq. (5) directly, note that all particles are reflected from the surface at a given time step with the temperature determined from the previous time step. Therefore, the net convective heat flux $(\Delta\dot{q})_t$ at time step t, representing the difference between incident and reflected particle energy per unit area, may be measured and stored,

$$(\Delta\dot{q})_t = (\dot{q}_{inc})_t - (\dot{q}_{refl})_t = (\dot{q}_{inc})_t - \left(\dot{N}_{inc}\frac{\zeta}{2}kT_s\right)_t \tag{6}$$

Equation (5) may be solved for the surface temperature corresponding to the next time step $(t+1)$ as follows:

$$(T_s)_{t+1} = \left(T_0^4 + \frac{\Delta\dot{q}}{\epsilon\sigma}\right)_t^{1/4} \tag{7}$$

This algorithm is very stable and leads to the appropriate surface temperature in just a few time steps. Time averaging the measured convective heat flux $\Delta\dot{q}$ is helpful to improve the statistical accuracy of the computed surface temperature T_s.

Dual-Node Surface Heat Transfer Model

An improved surface interaction model would account for heat transfer characteristics within the body itself. Heat transfer experienced by the solar panels and the HGA is of particular importance since these surface temperatures must remain below 393 and 408 K, respectively, during the aeropass maneuvers.[1] Effects of thermal conductivity across the plates, as well as heat capacity within the structure, may prove significant in determining surface temperatures. The following model is proposed for the heat transfer of the double-sided plates.

Table 1 Simulation flowfield specifications

Altitude, km	ρ_∞, kg/m^3	T_∞, K	m, g/mole	λ_∞, cm	M_∞	Kn_∞[a]	Scale, cm/cell
125	1.54×10^{-7}	198.0	42.2	94.8	37.71	0.256	7.86
130	4.97×10^{-8}	206.0	41.4	292.0	36.62	0.789	15.72
135	1.69×10^{-8}	215.0	40.4	852.0	35.41	2.303	15.72
140	6.13×10^{-9}	225.0	38.9	2340.0	33.96	6.324	31.44

[a]Based on high-gain antenna diameter of 370 cm, $Kn_\infty = \lambda_\infty / D_{HGA}$.

By neglecting transfer laterally along any surface, the researcher can model heat transfer through a plate structure with a two-node lumped-mass system where the nodes correspond, respectively, to the front (a) and back (b) sides of the plate facet. Energy conservation for each node must account for the convected energy due to particle impingement and reflection, the energy radiated at the node temperature, the energy conducted through the structure from one node to another, and the heat capacity stored within the node itself. By defining coefficients of conductivity κ and heat capacity c per unit area, the researcher can give the energy conservation equation for each node as follows;

$$\Delta \dot{q}_a(t) - \varepsilon_a \sigma (T_a^4 + T_0^4) - \kappa (T_a - T_b) = c_a \frac{dT_a}{dT}$$

$$\Delta q_b(t) - \varepsilon_b \sigma (T_b^4 + T_0^4) + \kappa (T_a - T_b) = c_b \frac{dT_b}{dt} \tag{8}$$

The convective heat fluxes $\Delta \dot{q}(t)$ are functions of time during the aeropass trajectory and are dependent on the freestream density and velocity. The deep-space temperature for radiation in this model is redefined and assumed equal to the initial surface temperature T_0 such that the panel is at radiative equilibrium before atmospheric entry.

This set of coupled differential equations may be solved numerically to assess each of the node temperatures T_a and T_b as they vary in time during the maneuver. However, due to limited computational resources, the particle simulation is capable of computing the flowfield at only a single point in time. Therefore, it is necessary to solve this set of equations to determine the maximum temperature at each node. These maxima will occur some time after the peak in the convective heat flux $\Delta \dot{q}(t)$ as a result of nonzero heat capacitance. If heat capacity were neglected ($c = 0$), Eqs. (8) would reduce to a set of polynomials independent of time. Indeed, if the thermal conductivity were infinite ($\kappa = \infty$), then the node temperatures would be equal ($T_a = T_b$) and the model would reduce to the radiative equilibrium model described earlier. However, as will be explored later, the effects of heat capacitance and thermal conductivity cannot be neglected.

Fully coupling this model into the particle simulation would require solving this set of equations repeatedly during the simulation for each of the surface facets on the body. Although this may be accomplished easily,[14] this degree of coupling was not employed in the present work. Instead, only the simple radiative equilibrium model was coupled into the simulation leading to surface temperatures T_s over the entire vehicle. However, the maximum net heat flux $\Delta \dot{q}_{max}$ as calculated in the simulation was used along with some assumed form for the transient function $\Delta \dot{q}(t)/\Delta \dot{q}_{max}$ to solve Eqs. (8) and to accurately reassess the solar panel temperatures T_a and T_b during the aeropass. Since the reassessed temperatures did not differ significantly from those determined from the simple model, the effect of these new temperatures on the flowfield was negligible

Surface Heating due to Chemical Reactions

It has been suggested that surface catalytic recombination of atomic oxygen and carbon monoxide, appearing in large quantities in the upper atmosphere of Venus, could significantly increase the heat load to the Magellan vehicle. Estimates of the maximum possible heating have been made and compared with the kinetic energy flux associated with flight conditions. It is possible to place an upper limit on the maximum possible heat transfer that could be released from these reactions by assuming that all of the available oxygen and carbon monoxide is consumed to form molecular oxygen and carbon dioxide. The following two exothermic reactions were considered[15]:

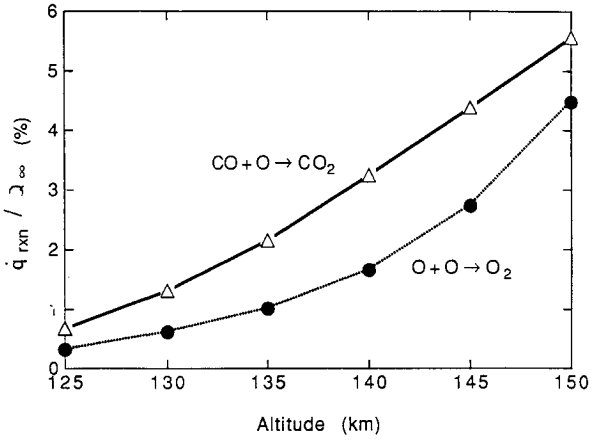

Fig. 2 Maximum possible heat flux resulting from chemical reactions on spacecraft surfaces.

$$O + CO \rightarrow CO_2 \quad (E_{rxn} = 8.75 \times 10^{-19} J) \tag{9}$$

$$O + O \rightarrow O_2 \quad (E_{rxn} = 8.21 \times 10^{-19} J) \tag{10}$$

Although reactions proceed through intermediates, these reactants and products represent the maximum possible heat release. Progression of one of the reactions will deplete reactants needed for the other reaction. Consequently, the peak energy flux due to reaction corresponds to complete consumption of reactants. Figure 2 presents estimates of the peak energy flux at several altitudes for a flight speed of 8600 m/s. The number densities of O and CO were employed as follows to compute the maximum possible energy flux due to chemical reaction $\dot{q}_{rxn}$:

$$\dot{q}_{rxn} = n_{rxn} u_\infty E_{rxn} \tag{11}$$

where n_{rxn} is the number density of the reactant species with the lowest concentration, and E_{rxn} is the chemical bond energy released during reaction and identified earlier.

These reaction energy fluxes are compared with the freestream kinetic energy flux Q_∞. The maximum $\dot{q}_{rxn}/Q_\infty$ ratio increases with altitude but remains below 3% at 140 km. Experience suggests that the surface catalycity of the solar panels will be considerably less than 100% such that reactions occurring at finite rates will not exhaust the supply of oxygen. These estimates of chemical energy flux are probably much larger than the vehicle will actually encounter. For this reason it is concluded that catalytic recombination may be ignored in the estimate of heat transfer to the surface of the Magellan spacecraft.

Simulation Results

For a spacecraft velocity of 8600 m/s at orbit periapsis, simulations were performed at altitudes of 125, 130, 135, and 140 km, which span over two orders of magnitude in atmospheric density. Specifications for each case are listed in Table 1 with day-side atmospheric data tabulated from Kliore et al.[16] Two simulations were performed at each altitude. The first used the tabulated freestream mean free path, whereas the second used an infinite mean free path representing free molecular flow. Comparisons between the two allowed the significance of rarefaction effects to be assessed. Other simulations were performed to assess the effects of coarse grid resolution and short upstream flow domain on solution results.

Since CO_2 dominates the atmospheric gas mixture, an effective intermolecular potential exponent of $\alpha = 5$ was used,[9] along with a fixed number of internal degrees of freedom ($\zeta_{int} = 3$) as noted earlier. The number of elastic collisions between each internally relaxing collision is fixed at five as dictated by the probability $P_{int} = 1/5$. Emissivity from all surfaces[17] is $\epsilon = 0.82$. Limited computational resources and the large number of cases investigated in the present study restricted the number of particles that could be employed in the simulation to just three particles per cell in the freestream. However, density gradients in the flowfield significantly increased the particle densities upstream of the body such that $0.6–1.2 \times 10^6$ particles existed in the flowfield at steady state. Employing roughly 6000 transient steps and 6000 steady-state sampling steps, the number of statistical samples was sufficiently large to yield accurate and meaningful solutions. The simulation could have employed ten times as many particles but would have required a tenfold increase in computational time per case, which was not warranted in the present study. Optimized for vector-processing architectures, the simulation requires roughly 1.2 μs of CPU time per particle per time step on a single-processor Cray Y-MP computer.

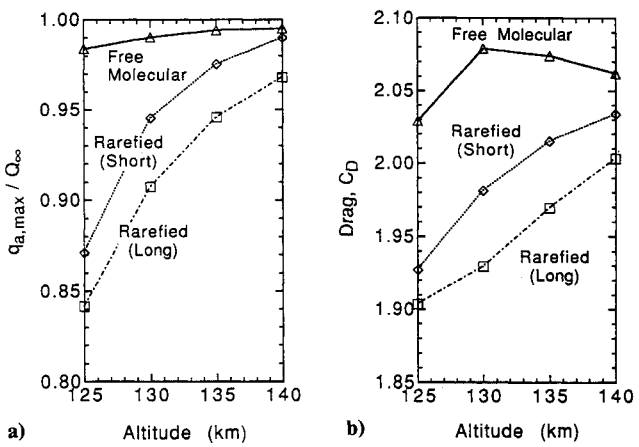

Fig. 3 Variation with altitude of aerodynamic coefficients from simulations of free molecular and rarefied flows employing long ($6D_{HGA}$) and short ($1.3D_{HGA}$) upstream domains: a) solar panel heating and b) vehicle drag.

Table 2 Simulation results

Altitude, km	$\Delta\dot{q}_{a,max}/Q$	C_D	T_{PAN},[a] K	T_{PAN},[b] K	λ_s, cells
125.0	0.842	1.904	816	876	0.92
130.0	0.907	1.930	627	587	1.24
135.0	0.946	1.969	484	395	3.49
140.0	0.968	2.003	377	307	7.96
125.0[c]	0.984	2.029	848	922	——
130.0[c]	0.990	2.079	641	609	——
135.0[c]	0.994	2.074	490	401	——
140.0[c]	0.995	2.062	380	309	——

[a]Radiative-equilibrium model, Eq. (7), with $\Delta\dot{q}_{PAN} = \Delta\dot{q}_{a,max}/2$.
[b]Dual-node surface heat transfer model, Eqs. (8), with $\tau = 250$ s and $T_0 = 250$ K.
[c]Free molecular simulation ($\lambda = \infty$).

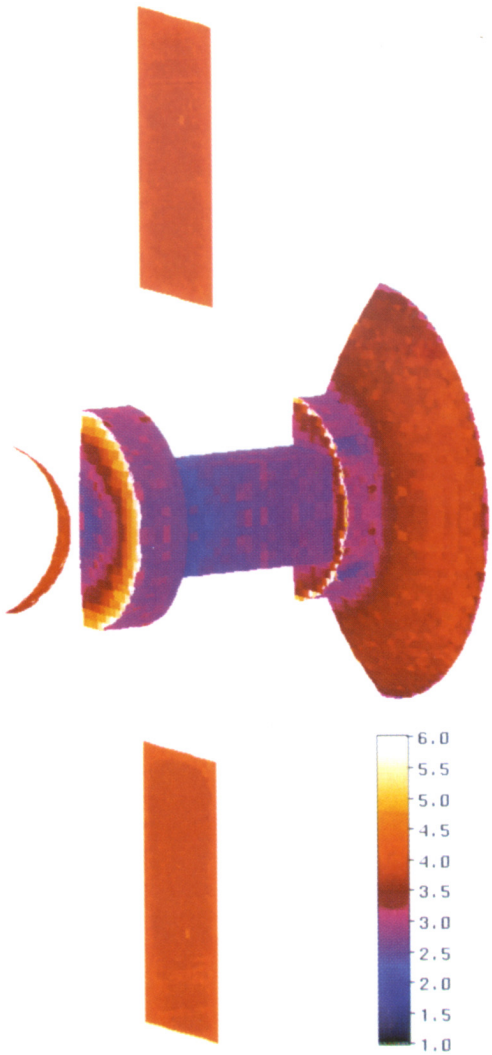

Fig. 4 Surface temperature ratio T_s/T_∞ computed with the radiative-equilibrium model for rarefied flow at 125-km altitude.

The results of each simulation are summarized in Table 2. Solution sensitivity to grid resolution and upstream domain is explored and observations regarding surface heating, drag, and flowfield features are discussed next.

Grid Resolution and Flow Domain

The cell resolution employed for the case at the 125-km altitude led to a stagnation mean free path of $\lambda_s = 0.92$ cells at the solar panel surface. A coarse grid was also used, doubling the cell size in each dimension to yield $\lambda_s = 0.46$ cells, for which the drag and heating estimates differed by less that 0.1% from the fine resolution results. At all of the other altitudes, λ_s readily exceeded one cell dimension as noted in Table 2. This indicates that the cell resolution employed throughout the present study was sufficiently fine to predict aerodynamics accurately.

Simulations were repeated at all altitudes using a short flow domain where the inflow boundary was located a distance of $1.3D_{HGA}$ upstream of the solar panels. As shown in Fig. 3, these results overpredicted drag and heating by as much as 2–4%. Accurate simulation therefore requires that the inflow boundary be located sufficiently far upstream to capture the influence of the body on the flow completely. For simulations at 140 km, Rault[5] employed an inflow boundary at a distance of less than $1.0D_{HGA}$ upstream of the solar panels, but nonetheless his work yielded drag results comparable to the present work. With such a limited

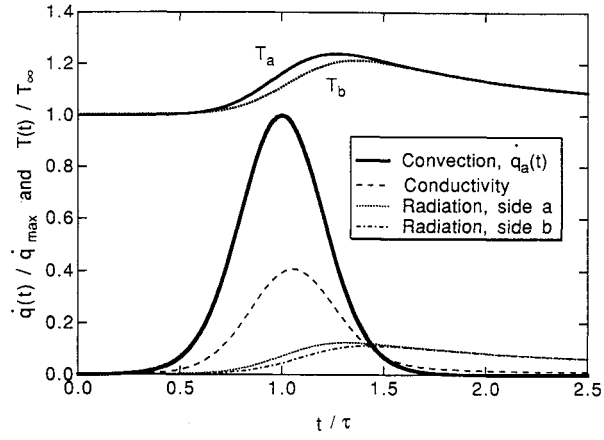

Fig. 5 Solar panel temperatures and heating from radiation, conductivity, and particle influx during aeropass using the dual-node surface heat transfer model (140 km, $\tau = 250$ s, $T_0 = 250$ K). Periapsis occurs at $t/\tau = 1$.

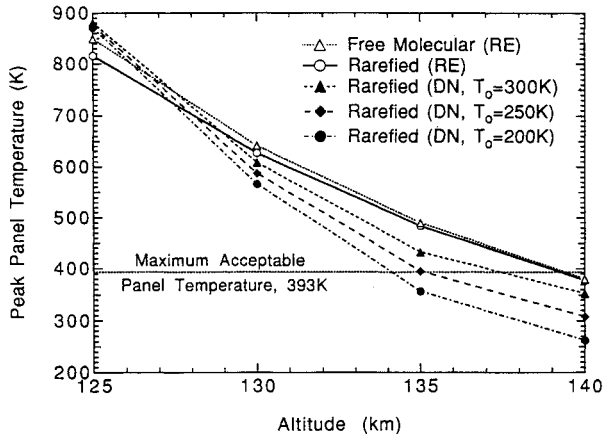

Fig. 6 Peak solar panel temperatures for rarefied and free molecular flows simulated with the radiative equilibrium (RE) model, Eq. (7), and compared with rarefied results from the dual-node (DN) model, Eqs. (8), with $\tau = 250$ s.

domain, however, poorer accuracy would be anticipated for heat transfer calculations, particularly at lower altitudes.

As expected for both heating and drag, rarefaction effects were more significant at lower altitudes, leading to values below the corresponding free molecular results. Peak heating in the free molecular cases was nearly equal to the bulk freestream translational energy Q_∞. Differences were due to particle reflection from the surface and an influx of particles reflected from other surfaces. For free molecular flow at 140 km, the simulation drag coefficient (2.062) agrees well with Schmitt's results[18] (2.081) using the analytic free molecular code, FREEMAC.

Radiative-Equilibrium Surface Heat Transfer

Surface temperatures, computed from the simulation with the simple radiative-equilibrium model, are presented in Fig. 4 for rarefied flow at 125 km. As expected, temperatures were greatest on the solar panels, the HGA, and the SRM for each case, attaining values between roughly two and six times the freestream temperature T_∞. Other body surfaces were relatively cool ($T_s/T_\infty < 1$) since they were mostly "shaded" from the freestream flow by other body components. The annular ring on the edge of the BUS face that was exposed to the direct flow was quite hot since this surface radiated in only one direction. Fortunately, this is not a delicate surface, and the excessive temperature is of little concern.

Dual-Node Surface Heat Transfer

The particle energy flux into the solar panel, resulting from each simulation, was input into the dual-node heat transfer model. The coupled differential equations (8) were integrated numerically over the duration of the heating pulse to yield more appropriate estimates of solar panel temperatures. Thermal coefficients[17] accounted for material densities and thickness and included conductivity through the panels given by $\kappa = 59.50$ W/m^2-K and heat capacities given by $c_a = 2037.8$ J/m^2-K for the diodes on the upstream side of the solar panel and $c_b = 1506.4$ J/m^2-K for the downstream side. The form of the heating flux pulse on the front of the solar panel was taken from Scott[17] and was fit to the following equation, shown as a solid line in Fig. 5,

$$\Delta\dot{q}_a(\tilde{t}) / \Delta\dot{q}_{a,\max} = \frac{(1 - \cos \pi\tilde{t})}{2} \exp(-2 - 2\cos \pi\tilde{t}) \quad (12)$$

where $\tilde{t} \equiv t/\tau$ is time normalized by the heating pulse duration τ, and $\Delta\dot{q}_{a,\max}$ is taken as the net convective heat flux per unit frontal area from the steady-state particle simulation solution. Since particle incidence on the back of the solar panel was negligible compared with that on the front, it was assumed that $\Delta\dot{q}_b(\tilde{t}) = 0$ and $\Delta\dot{q}_{a,\max} = 2\Delta\dot{q}_{PAN}$ where $\Delta\dot{q}_{PAN}$ is the heat flux per unit of total solar panel surface area (front and back sides).

The initial surface temperature of the solar panels was estimated to be $T_0 = 250$ K before the first aeropass maneuver of duration $\tau = 250$ s. Figure 5 depicts the transient energy fluxes and surface temperatures during the aeropass at 140 km under these conditions. Note that each temperature reached its maximum value after the peak in the convective heat flux $\Delta\dot{q}_a$ (at periapsis, time, $(\tilde{t}) = 1$) as a result of nonzero heat capacity c.

Sensitivity of transient surface temperature T_s to the initial temperature T_0 is demonstrated for the rarefied results at all altitudes in Fig. 6. Clearly, the acceptable entry altitudes predicted by the simulation are greatly influenced by the assumed surface heat transfer model. Surface temperatures from the simple radiative equilibrium model are also shown in this figure and are much higher than those from the more sophisticated heat transfer model, except at the lowest altitude. Nonetheless, if the reassessed temperatures were coupled back into the simulation, the resulting peak convective heat flux $\Delta\dot{q}_{a,\max}$ predicted by the simulation would

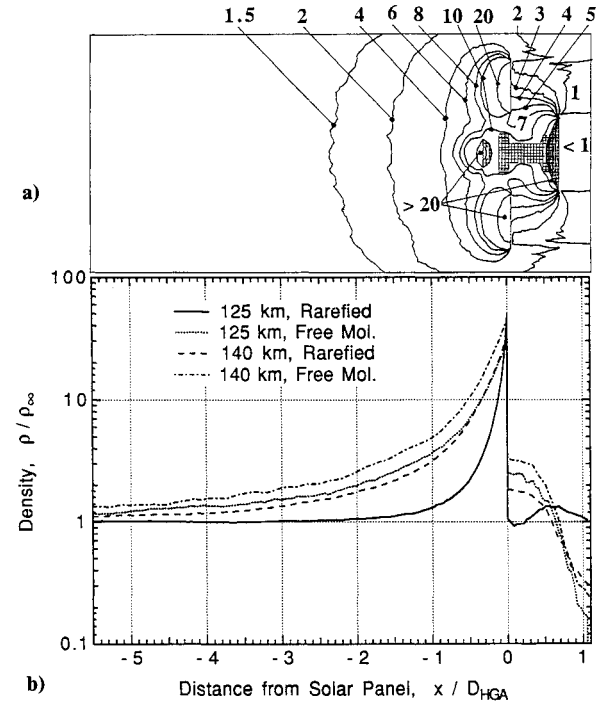

Fig. 7 Flowfield density ρ/ρ_∞: a) contours for rarefied flow at 135-km altitude and b) plot of ρ/ρ_∞ along the stagnation streamline at the center of the solar panel.

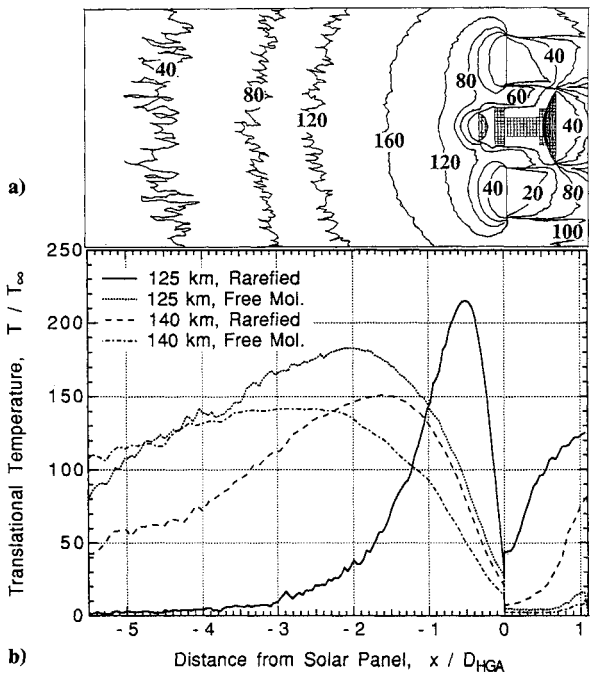

Fig. 8 Flowfield translational temperature T/T_∞: a) contours for rarefied flow at 135-km altitude and b) plot of T/T_∞ along the stagnation streamline at the center of the solar panel.

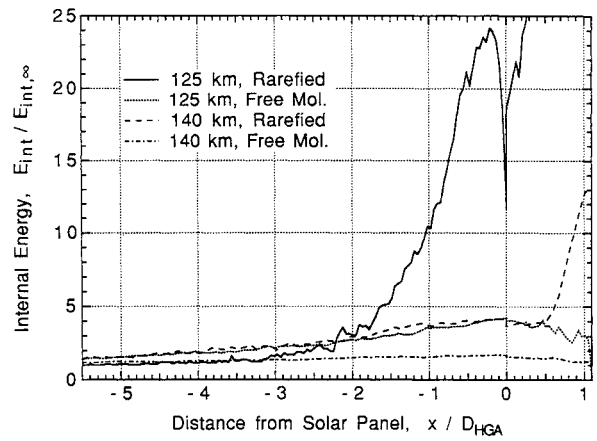

Fig. 9 Molecular internal energy $E_{int}/E_{int,\infty}$ along the stagnation streamline at the center of the solar panel.

not have differed significantly from those listed in Table 2. This is because, under such rarefied conditions, $\Delta\dot{q}_{a\max}$ was primarily dependent on the freestream density and velocity rather than on the flowfield temperatures in the vicinity of the surface.

Flowfield Density

As shown in Fig. 7a at 135-km altitude, steady-state densities that exceed the freestream value extend far upstream of the body as a result of significant diffusion of particles that reflected from body surfaces. Likewise, particles reflecting from the HGA diffused into the flowfield behind the solar panel, leading to densities exceeding the freestream value. Density profiles along the stagnation streamline at the center of the solar panel are presented in Fig. 7b at altitudes of 125 and 140 km. The distinction between rarefied and free molecular results is much greater at the lower altitude.

Flowfield Temperature

In particle methods, flowfield translational temperature is defined by the variance of the velocity distribution for each cell. Contours of temperature ratio (T/T_∞) on the symmetry plane defined by the solar panel axis are shown in Fig. 8a for rarefied flow at 135-km altitude. Temperature along the stagnation streamline at the center of the solar panels is indicated in Fig. 8b to demonstrate differences between rarefied and free molecular flows. The temperature ratio rose two orders of magnitude even for the free molecular flows where there are no collisions to heat the incoming gas. Nonetheless, the total translational energy of the flow upstream of the spacecraft remained roughly equal to the freestream value.

This paradox results from the non-Maxwellian nature of the velocity distribution in nonequilibrium rarefied flows. Each cell in the flowfield ahead of the solar panel contained particles of two distinct types: those that came from the freestream with high velocity and low temperature and those that had reflected from the panel and were diffusing upstream with essentially zero velocity and with a temperature corresponding to the surface. In the absence of molecular collisions, the resulting velocity distribution for each cell was bimodal. The variance of this distribution was consequently very high, even though the variance of each hump in the distribution was low as expected for freestream or surface temperatures. It is apparent in Fig. 8b that molecular collisions led to a higher and narrower temperature profile at 125-km altitude than the profile that occurred in the corresponding free molecular case. Differences between rarefied and free molecular profiles are less pronounced at 140-km altitude. Nonetheless, these plots indicate that the influence of the body on the flow extends far upstream, necessitating the use of a large upstream simulation domain.

Effects of particle collisions are most evident in plots of molecular internal energy E_{int} in Fig. 9. Particles attained the internal energy associated with the temperature of the fully accommodating surfaces from which they reflected. Particles diffusing upstream and downstream carried this internal energy, leading to fairly invariant plots for free molecular flows in the figure. However, molecular collisions with energetic freestream particles led to greatly increased internal energies ahead of the solar panels for rarefied flow at 125 km. This behavior is far less notable for rarefied flow at 140 km, which indicates that this flow was nearly free molecular.

Concluding Remarks

Differences between free molecular and rarefied flowfields and their effects on surface heating and drag were assessed through a particle simulation of aeropass maneuvers of the Magellan spacecraft at high altitudes in the atmosphere of Venus. Simulations of rarefied flow employed the finite mean free path appropriate for each altitude; free molecular flows employed an infinite mean free path. The simulation grids were sufficiently fine to yield accurate solutions. Simulations that employed upstream domains of insufficient length overpredicted heating and drag.

Surface temperatures that were computed directly in the simulation, assuming radiative equilibrium, were typically higher than those computed in an uncoupled manner with the dual-node model employing the net particle energy flux determined from the simulation and accounting for material heat capacity and thermal conductivity. For each heat transfer model, the resulting surface temperatures and drag were lower in the rarefied flow than in the free molecule flow, although these differences were small above 135 km. It is noteworthy that at the lower altitudes surface heating exceeds the surface temperature limitations specified for the solar panels.

This study concludes that the flowfield about the Magellan spacecraft during its aeropass maneuvers at acceptable altitudes was nearly free molecular. At slightly lower altitudes, which led to excessive surface heating due to increased atmospheric density, molecular collisions significantly affected the flow as captured with the particle simulation method.

Acknowledgments

Support of NASA Ames Research Center and the Numerical Aerodynamic Simulation facility is appreciated. This work was sponsored in part (for the first author) by NASA Grant NCC2-582. The authors gratefully acknowledge the assistance and technical

support of Michael Tauber (NASA Ames), Daniel Lyons (JPL), Durwin Schmitt and Owen Scott (Martin-Marietta Corporation), and Van Carey and Franklin Hurlbut (University of California, Berkeley). Special thanks to Jeffrey McDonald, formerly with Eloret Institute at NASA Ames (now with MasPar Computer Corporation), and Michael Fallavollita (Stanford University) for assistance in using the simulation and postprocessing visualization codes.

References

[1]Lyons, D. T., Sjogren, W., Johnson, W. T. K., Schmitt, D., and McRonald, A., "Aerospace Magellan," American Astronomical Society, AAS Paper 91-420, Aug. 1991.

[2]Fredo, R. M., and Kaplan, M. H., "Procedure for Obtaining Aerodynamic Properties of Spacecraft," *Journal of Spacecraft and Rockets,* Vol. 18, No. 4, 1981, pp. 367–373.

[3]Baganoff, D., and McDonald, J. D., "A Collision-Selection Rule for a Particle Simulation Method Suited to Vector Computers," *Physics of Fluids A,* Vol. 2, No. 7, 1990, pp. 1248–1259.

[4]McDonald, J. D., "A Computationally Efficient Particle Simulation Method Suited to Vector Computer Architectures," Ph.D. Thesis, Stanford Univ., Stanford, CA, 1989.

[5]Rault, D. F. G., "Aerodynamics Characteristics of Magellan Spacecraft in Venus Upper Atmosphere," AIAA Paper 93-0724, Jan. 1993.

[6]Bird, G. A., *Molecular Gas Dynamics,* Clarendon Press, Oxford, England, UK, 1976.

[7]Haas, B. L., "Thermochemistry Models Applicable to a Vectorized Particle Simulation," Ph.D. Thesis, Stanford Univ., Stanford, CA, 1990.

[8]Haas, B. L., "Models of Energy-Exchange Mechanics Applicable to a Particle Simulation of Reactive Flow," *Journal of Thermophysics and Heat Transfer,* Vol. 6, No. 2, 1992, pp. 200–207.

[9]Bird, G. A., "Monte-Carlo Simulation in an Engineering Context," *Rarefied Gas Dynamics,* 12th International Symposium on Rarefied Gas Dynamics, Charlottesville, VA, July 1980, pp. 239–255.

[10]Borgnakke, C., and Larsen, P. S., "Statistical Collision Model for Monte Carlo Simulation of Polyatomic Gas Mixture," *Journal of Computational Physics,* Vol. 18, No. 4, 1975, pp. 405–420.

[11]Moss, J. M., and Bird, G. A., "Direct Simulation of Transitional Flow for Hypersonic Reentry Conditions," *Thermal Design of the Aeroassisted Orbital Transfer Vehicles,* edited by H. F. Nelson, Vol. 96, Progress in Astronautics and Aeronautics, AIAA, New York, 1985; see also AIAA Paper 84-0223, Jan. 1984.

[12]Bird, G. A., "Definition of Mean Free Path for Real Gases," *Physics of Fluids,* Vol. 26, No. 11, 1983, pp. 3222, 3223.

[13]Carey, V., and Hurlbut, F., private communication, Univ. of California, Berkeley, Berkeley, CA, Oct. 1991.

[14]Haas, B. L., "Particle Simulation of Satellite Aerobraking with Coupled Surface Heat Transfer," 18th International Symposium on Rarefied Gas Dynamics, Vancouver, BC, Canada, July 1992 (to be published).

[15]Von Zahn, U., Kumar, S., Nieman, H., and Prinn, R., *Venus,* Univ. of Arizona Press, Tucson, AZ, 1983.

[16]Kliore, A. J., Moroz, V. I., and Keating, G. M., *Venus International Reference Atmosphere,* Vol. 5, No. 11, Pergamon, Oxford, England, UK, 1986, pp. 142–148.

[17]Scott, O., private communication, Martin-Marietta Astronautics Corp., Denver, CO, Oct. 1991.

[18]Schmitt, D., private communication, Martin-Marietta Astronautics Corp., Denver, CO, June 1992.

Gerald T. Chrusciel
Associate Editor